AD-A060 121 NAVAL OCEAN SYSTEMS CENTER SAN DIEGO CA F/G 8/10
THE EFFECT OF UPDATE RANDOMIZATION ON REVGEN OUTPUT: BROADBAND --ETC(U)
AUG 78 J G MELVILLE, M E STEGMAN

UNCLASSIFIED NOSC/TR-292 NL

1 OF 1
AD
A060121

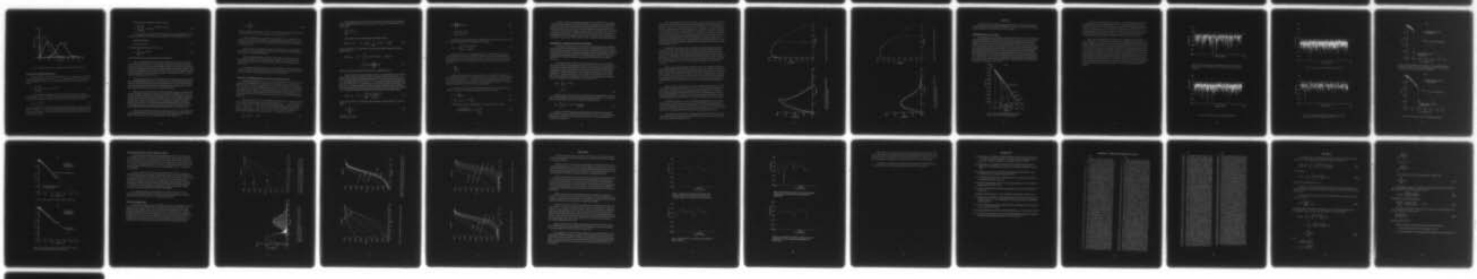

END
DATE
FILMED
12-78
DDC

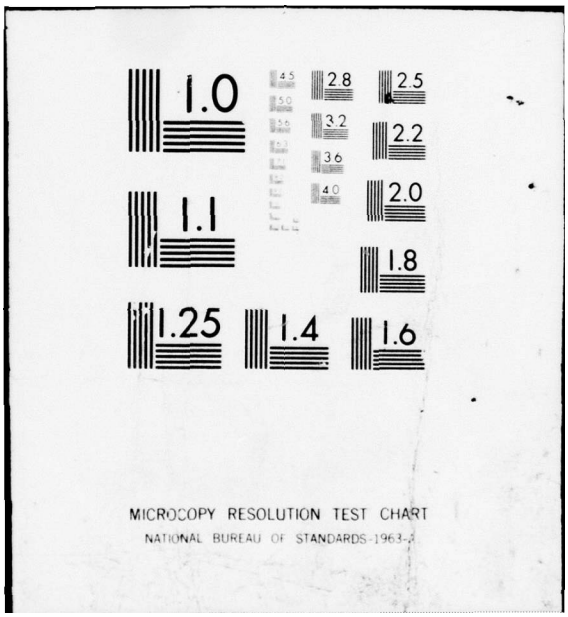
1.0
1.1
1.25
1.4
1.6
1.8
2.0
2.2
2.5
2.8
3.2
3.6
4.0
4.5
5.0
MICROCOPY RESOLUTION TEST CHART
NATIONAL BUREAU OF STANDARDS-1963-A

NOSC

(13) LEVEL II

NOSC TR 292

Technical Report 292

THE EFFECT OF UPDATE RANDOMIZATION ON REVGEN OUTPUT: BROADBAND ENERGY DETECTOR

J. G. Melville and M. E. Stegman

31 August 1978

Final Report: April - August 1978

Prepared For
Naval Sea Systems Command

APPROVED FOR PUBLIC RELEASE; DISTRIBUTION UNLIMITED

NAVAL OCEAN SYSTEMS CENTER
SAN DIEGO, CALIFORNIA 92152

NAVAL OCEAN SYSTEMS CENTER, SAN DIEGO, CA 92152

AN ACTIVITY OF THE NAVAL MATERIAL COMMAND

RR GAVAZZI, CAPT, USN
Commander

HL BLOOD
Technical Director

ADMINISTRATIVE INFORMATION

The work presented in this report was performed during the months of April through August 1978 and sponsored by the ALWT Project Office of the Naval Sea Systems Command.

Released by
D. M. Chabries, Head
Weapons Technology Division

Under authority of
D. A. Kunz, Head
Fleet Engineering Department

UNCLASSIFIED

SECURITY CLASSIFICATION OF THIS PAGE *(When Data Entered)*

REPORT DOCUMENTATION PAGE

READ INSTRUCTIONS BEFORE COMPLETING FORM

1. REPORT NUMBER: NOSC TR-292	2. GOVT ACCESSION NO.
3. RECIPIENT'S CATALOG NUMBER	
4. TITLE *(and Subtitle)*: THE EFFECT OF UPDATE RANDOMIZATION ON REVGEN OUTPUT: BROADBAND ENERGY DETECTOR	5. TYPE OF REPORT & PERIOD COVERED: Final Report: April–August 1978
6. PERFORMING ORG. REPORT NUMBER	
7. AUTHOR(s): J. G. Melville, M. E. Stegman	8. CONTRACT OR GRANT NUMBER(s)
9. PERFORMING ORGANIZATION NAME AND ADDRESS: Naval Ocean Systems Center, San Diego, CA 92152	10. PROGRAM ELEMENT, PROJECT, TASK AREA & WORK UNIT NUMBERS
11. CONTROLLING OFFICE NAME AND ADDRESS: Naval Sea Systems Command, Washington, D.C.	12. REPORT DATE: 31 August 1978
	13. NUMBER OF PAGES: 37
14. MONITORING AGENCY NAME & ADDRESS *(if different from Controlling Office)*	15. SECURITY CLASS. *(of this report)*: Unclassified
	15a. DECLASSIFICATION/DOWNGRADING SCHEDULE

16. DISTRIBUTION STATEMENT *(of this Report)*

Approved for public release, distribution unlimited.

(11) 31 Aug 78

(12) 47 p.

17. DISTRIBUTION STATEMENT *(of the abstract entered in Block 20, if different from Report)*

18. SUPPLEMENTARY NOTES

19. KEY WORDS *(Continue on reverse side if necessary and identify by block number)*

Reverberation
Broadband
Detection
Threshold Effects
Rayleigh Scattering

20. ABSTRACT *(Continue on reverse side if necessary and identify by block number)*

Current advancements in computer simulation of ocean reverberation include the realtime implementation of REVGEN (Reverberation Generator). The REVGEN algorithm which determines the randomization and number of update components can significantly affect the form of the reverberation return and correspondingly alter the false alarm and detection statistics for the response of a broadband energy detector. When the updates are limited and assigned constant amplitudes, there is a reduction in the probability of high intensity returns which, in turn, affect detector performance in two ways:

DD FORM 1 JAN 73 1473 EDITION OF 1 NOV 65 IS OBSOLETE
S/N 0102-014-6601

UNCLASSIFIED

SECURITY CLASSIFICATION OF THIS PAGE *(When Data Entered)*

393 159

20. (Continued).

1. For a given signal-to-noise ratio, a signal produced with updates of constant magnitude will result in erroneously low probability of false alarm (PFA).

2. These lowered PFA rates cause incorrect placement of detection thresholds which then yield erroneously high probabilities of detection.

Both theoretical calculations and computer simulation show that increasing the number of updates resolves the statistical disparity. However, the reverberation algorithm which randomizes the update amplitudes according to a Rayleigh distribution is seen to yield the proper statistics independent of the number of updates used in the simulation. This decoupling of the detection statistics from the update algorithm may, for some simulation applications, provide the opportunity to reduce REVGEN computational requirements.

SUMMARY

OBJECTIVE

To illustrate the effect of update randomization on the envelope statistics of REVGEN reverberation returns and to examine the corresponding probabilities of false alarm and detection for the response of a broadband energy detector.

RESULTS

When updates are limited and assigned constant magnitudes, the form of the reverberation envelope is altered by a reduction in the probability of obtaining high intensity returns. This affects the detection statistics for a broadband energy detector in two ways:

1. For a given signal-to-noise ratio, a signal produced with updates of constant magnitude will result in erroneously low probability of false alarm.

2. These lowered PFA rates cause incorrect placement of detection thresholds which, in turn, yield erroneously high probability of detection.

RECOMMENDATIONS

Both theoretical calculations and computer simulation show that increasing the number of updates resolves the statistical disparity. However, when the update amplitudes are randomized according to a Rayleigh distribution, the proper statistics are obtained independent of the number of updates used in the simulation.

CONTENTS

INTRODUCTION

The rapid development of microelectronic technology has greatly enhanced the signal processing and self-guidance capabilities of lightweight torpedoes. To accurately evaluate the performance of new torpedo designs, including such features as matched filter processing and coherent signal processing, requires a corresponding increase in sophistication of the NOSC weapons simulation facility. A major element of that improvement is the realtime implementation of REVGEN (Reverberation Generator),[1] a digital simulation of ocean reverberation.

The requirement that REVGEN run in realtime on the present NOSC, UNIVAC 1110 based hybrid simulator has necessitated several simplifying alterations to the original REVGEN concept. This note examines the effects of these simplifications on the statistics of the REVGEN output.

The physical derivations of the original REVGEN process and of the version currently operative on the NOSC Hybrid Simulator have already received ample documentation.[1,2,3] However, for the purposes of a brief review and to establish notation, the basics of this process are here outlined.

The output of REVGEN can be written in terms of the following matrix equation, i.e.,

$$\underset{\sim}{Y} = B\underset{\sim}{X}$$

$$Y_J = \sum_{L=0}^{N-1} B_{J,L}\, X_L \tag{1}$$

where $\underset{\sim}{X}$ represents a sampled vector of the transmit pulse and $\underset{\sim}{Y}$ correspondingly represents the return echo. If $\underset{\sim}{X}$ and $\underset{\sim}{Y}$ sample the time series at rates equal to the inverse of twice the respective band widths (w_Y, w_X) of the transmit pulse and return echo, it can be shown that the B-matrix contains all the information concerning the ocean medium that is available to that specific ping-echo process.[1]

The B-matrix is calculated from the doppler-density matrix D in the following way[1]

$$B_{J,L} = \sum_{M=0}^{N-1} D_{J-L,M}\, e^{-2\pi jML/N} \tag{2}$$

where N is the number of transmit pulse samples in $\underset{\sim}{X}$, $L_{max} = N - 1$, and J indexes the time of the echo return. The doppler-density matrix has elements that correspond to different range and doppler returns in the echo. The rows of $D_{J,L}$ represent the spectral distribution of the scatterers at a particular range slice J.

To conform to the necessary sample rates outlined above, the adjacent elements of doppler-density matrix must be separated by $1/2w$ in range and $1/2\tau p$ (τp = ping length) in frequency.

The present simulation generates reverberation in a three-step process. First the doppler-density matrix is calculated from data defining the ocean environment and the torpedo state (i.e., velocity, beam patterns, etc.). Second, the B-matrix is formed as outlined in Equation (2). Third, the echo is generated from the B-matrix and the transmit pulse as given in Equation (1).

To use this optimally accurate REVGEN calculation in the weapon simulator, the rows of the D_{JL} must be computed* in realtime. For typical conditions this would require 256 rows to 256 doppler-density values to be calculated each pulse length τp. The current capability of the simulator is to calculate 1 row of 256 values per time τp.

The disparity between the optimum number range slices of D_{JL} per pulse length and the fact that only one can be calculated has led to certain "update" algorithms which serve to fill in parts of the doppler-density matrix without resorting to the lengthy direct calculation of the ocean algorithm.

Figure 1 illustrates how this update procedure is accomplished. Figure 1(a) shows a doppler-density matrix which has been completely filled in by performing the ocean algorithm calculation for each range slice (separated in time by $1/2w$). By comparison, Figure 1(b) shows a similar matrix for which the ocean algorithm has been called only once per pulse length.

From experience it is known that the average magnitudes of each element in the rows of D_{JL} do not change much during one pulse length (i.e., $|\overline{D_{J,L}}| \approx |\overline{D_{J+N,L}}|$ where N is the number of range slices per pulse length).

Since the average magnitude does not change rapidly with range, the only difference in a particular column from one row to the next will be a randomization in phase of the form $e^{i\phi}$ where ϕ is uniformly distributed between zero and 2π. Figure 1(c) shows a matrix that has been filled in using this approximation. The first row in each pulse length has been calculated using the ocean algorithm. The rows marked with a "u" have been formed using the magnitudes from the first row and a random phase for each update bin. The total number of rows per pulse length is referred to as the number of updates per pulse length. The current NOSC realtime simulator is capable of processing 8 updates per pulse length. Since a ping may typically have 256 range slices, this is still far from the theoretical optimum.

---

*The ocean algorithm which is used to construct the NOSC-REVGEN doppler-density matrix partitions up the ocean into cells corresponding in range and doppler and then calculates the magnitude of the return from each cell according to the standard sonar equations.[3] These values are then each given complex random phase and loaded into the appropriate element of the matrix.

This procedure departs from the true form of the doppler density in that it assigns a deterministic magnitude (calculated from the sonar equations) to the elements of D_{JL} while in reality those values are stochastic in nature. In the case where many scatters are participating in an instantaneous echo return it has been shown (in Schwartz[4] for example) that the magnitude of the return has a Rayleigh distribution.

The above process would be more realistic if, after the mean intensity I_{JL} from an ocean cell was determined from the sonar equations, the magnitude of D_{JL} be randomly chosen from a population of Rayleigh random numbers having the mean power I_{JL}.

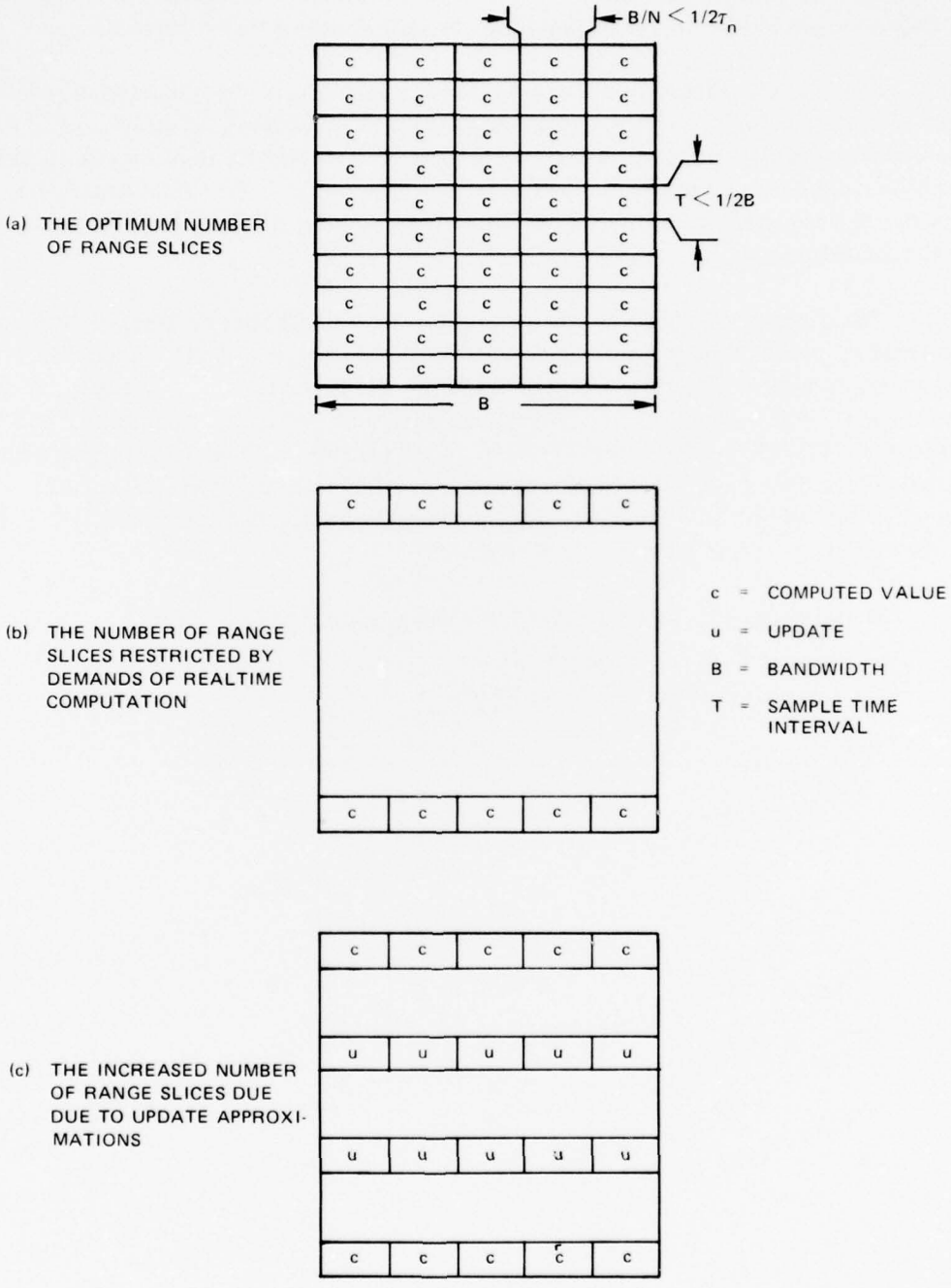

Figure 1. Doppler-density matrix representations.

At this point several important questions arise. First, how will this under sampling of DJL affect the results of a torpedo simulation run? Second, for cases where the change in performance is significant, is there a different update algorithm, compatible with realtime operation on the hybrid simulator, that could be used to improve performance?

The answers to these questions are quite dependent upon the type of signal processing used to analyze the reverberation return. As noted by Princehouse[1] the specifications for the bin dimension in DJL are based on a matched filter processor whose transmit pulse simultaneously contains optimum resolution in both range and doppler. In situations using other processors, a reduction in the update number may be possible without affecting the output of the simulation run.

The remainder of this note will demonstrate how the above two questions can be answered by studying the response of a simple broadband energy detector to REVGEN output generated using several different update algorithms. It will first be shown that the statistics of the REVGEN signal-detector process can be represented in analytical form. The statistics for the fully updated, properly randomized process (i.e., real world) are also presented in closed form. From these expressions, probability of false alarm statistics, receiver operating characteristic curves, and power curves will be generated to demonstrate the effect of the update algorithms on system performance.

These results will also be demonstrated using actual REVGEN data.

THEORY

This section develops techniques to statistically characterize 1) the reverberation return from point scatterers in an ideal ocean; 2) the corresponding REVGEN output; 3) the modified REVGEN output and its application to the theory for two dimensional random walks; and 4) the response of a broadband energy detector to real and simulated reverberation data.

ENVELOPE STATISTICS FOR A POINT SCATTERING MODEL

The physical model upon which REVGEN is based assumes that the reverberation is the sum of individual echoes from point scatterers in the ocean medium.[1] The expressions describing the reflected return from such a random medium of point scatterers are well known and adequately reviewed in Ol'shevskii[4] as well as standard texts on communications theory.[5,6]

The present note follows chapter 5 of Schwartz[6] to introduce the statistics of signal propagation through so-called random or fading media.

For a medium composed of randomly placed, stationary point scatterers of amplitude a_L, the envelope of the reverberation signal has the form

$$r = \sum_L a_L \, e^{i\theta L} \tag{3}$$

where θ_L is determined by the location of the L^{th} scatterer in the medium. Due to the random placement of the scatterers, θ_L is a random number with uniform distribution. When no one scatterer dominates the return (i.e., all the a_L's are of comparable strength), the distribution of the magnitude of r can be shown to have the following form.

$$f_r(r) = \frac{r}{\sigma^2} \, e^{-r^2/2\sigma^2} \tag{4}$$

where

$$2\sigma^2 = \sum \sigma_{a_L}^2 .$$

This distribution, named after Lord Rayleigh who originally solved the problem in 1880,[7] has the following properties

1. The most probable value of $r = \sigma$ (5)

2. $E(r) = (\pi/2)^{1/2} \, \sigma$ (6)

3. Median value of $r = 1.185 \, \sigma$ (7)

4. $E(r^2) = power = 2\sigma^2$ (8)

5. The variance $E((E(r) - r)^2) = (2 - \pi/2)^2$ (9)

6. Probability of r exceeding a threshold $r_T = e^{-r^2/2\sigma^2}$ (10)

The derivation of this distribution was based in part on the central limit theorem and therefore is not valid for cases where the number of scatterers is small. As noted by Princehouse,[8] a typical* sonar might ensonify approximately 4×10^7 scatterers. For most pulse lengths this would insure a large number of scatterers in any instantaneous scattering volume.

The previous paragraphs describe the statistical character of the echo return from randomly placed scatterers of approximately equal amplitude. Of importance to detection theory is the form of the return when there is one particular dominant component in the scattering field (e.g., a target).

When a component of amplitude A is added to the previously defined group of scatterers the envelope of the return signal has the following distribution.[9]

$$f(r) = \frac{r}{\sigma^2} e^{-(r^2 + A^2)/2\sigma^2} I_0(rA/\sigma^2) \tag{11}$$

where I_0 is the modified Bessel function of the first kind and zero order. This is known as a Rician distribution and can be seen to be identical to the Rayleigh distribution (Equation (4)) when $A = 0$.

In the limit that $rA \gg \sigma^2$ it can be shown that

$$f(r) \approx \frac{1}{\sqrt{2\pi\sigma^2}} e^{-(r - A)^2/2\sigma^2} \tag{12}$$

which has the form of a Gaussian distribution centered at the magnitude of the specular component A.

Figure 2 shows this transition from Rayleigh to offset Gaussian distribution by plotting Rician distributions for signal-to-noise ratios of $-\infty$ dB (Rayleigh), 1 dB (intermediate), and 10 dB (off-centered Gaussian). The signal-to-noise ratio (power) has the form

$$\frac{\textit{Power target}}{\textit{Power Reverberation}} = \frac{A^2}{2\sigma^2} \tag{13}$$

The foregoing has reviewed the statistical nature of signals that would be received from an idealized but real ocean environment. Next, statistics of the REVGEN reverberation signal will be determined.

*15-degree beam width and 4000-meter range.

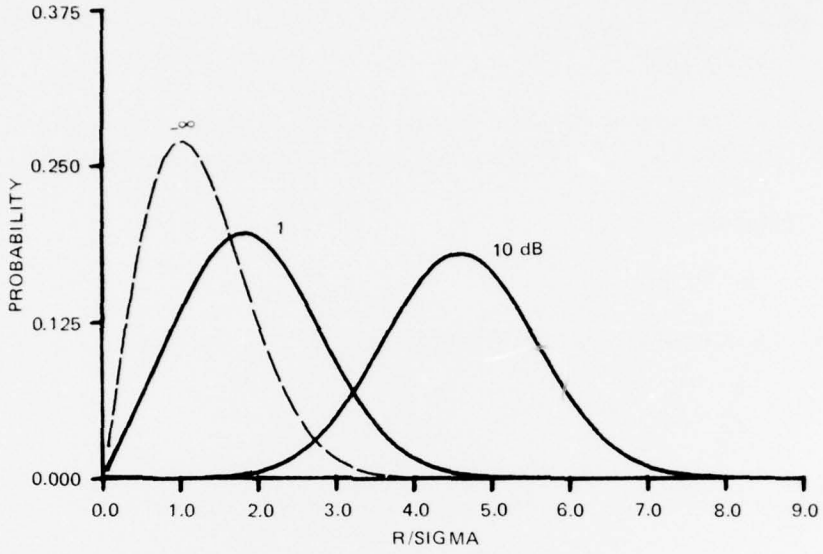

Figure 2. Rayleigh and Rician (off-set Gaussian) distributions for SNR of 1 and 10 dB.

ENVELOPE STATISTICS FOR REVGEN

Given the doppler-density matrix, REVGEN produces a complex time series (demodulated) corresponding to the reverberation echo. From Equations (1) and (2) an expression for the output time function can be written which explicitly shows the doppler-density matrix.

$$Y_J = \sum_{L=0}^{N-1} \sum_{M=0}^{N-1} x_L \, D_{J-L,M} \, e^{-i2\pi ML/N} \tag{14}$$

A few observations regarding the doppler-density matrix will serve to simplify the form of Equation (12). As the number of ocean scatterers falling within each range and doppler interval becomes large, the elements $D_{J,L}$ become random variables of the form

$$D_{J,L} = d_{J,L} \, e^{i\phi_{J,L}} \tag{15}$$

where $d_{J,L}$ is distributed according to a Rayleigh distribution and $\phi_{J,L}$ is a uniform distribution over the limits $(0, 2\pi)$. This follows from the discussion of Rayleigh statistics presented previously. For the case of a uniform spatial distribution of scatterers, the values of $D_{J,L}$ are statistically independent.

With this notation, Equation (14) can be written

$$Y_J = \sum_{L=0}^{N-1} \sum_{M=0}^{N-1} x_L \, d_{J-L,M} \, e^{-J(2\pi ML/N - \phi_{J-L,M})} \tag{16}$$

For the purpose of statistical analysis it is noted that the exponential factor in Equation (16) is equivalent to $e^{i\theta_{L,M}}$ where $\theta_{L,M}$ is distributed in the same manner as $\phi_{J,L}$.

Making the definition

$$a_{J,L,M} = x_L \, d_{J-L,M}, \tag{17}$$

the following expression may be written for Y_J:

$$Y_J = \sum_{L,M} a_{J,L,M} \, e^{i\theta_{L,M}}. \tag{18}$$

This has been made to have the same structure as Equation (3).

There is a fundamental difference, however, between the values $a_{J,L,M}$ of Equation (18) and the a_L's of Equation (3). The subscript L in Equation (3) labels each scattering center in the section of the ocean being investigated (as noted before, this is a very large number for most sonar applications), while $a_{J,L,M}$ labels elements in a computer simulation. Due to practical considerations such as the time and cost of computation, the number of elements summed in Equation (18) must be kept to a minimum. This requires that one $a_{J,L,M}$ represents the scattering from many of the a_L's.

If when computing the $a_{J,L,M}$'s of Equation (17), the values $d_{J,M}$ are chosen according to a Rayleigh distribution, then $|Y_J|$ will have the proper statistical distribution independent of the number of elements used in the computation. In this case, Equation (18) is the sum of complex normal random variables and is therefore itself a complex random variable having magnitudes distributed according to a Rayleigh distribution.

However, this is not always the case. When the elements $a_{J,L,M}$ are not random variables but are fixed according to a deterministic calculation (for example based on the mean intensity of scatterers from within a certain volume), then the only randomness in Y_J occurs in $\theta_{L,M}$. This in turn alters the statistical distribution of $|Y_J|$. As the number of significant components in Equation (18) becomes large, $|Y_J|$ will approach a Rayleigh distribution. However, when the number of components is small, significant differences can be noted. From Equation (18) it can be seen that the number of components is equal to the product of the number of updates per pulse length and the number of non-zero frequency bins.

Under some conditions there is only one filled frequency bin in a reverberation simulation. When REVGEN is operating in its update mode with 8 updates per pulse length, Y_J would be formed from the sum of 8 complex phasors of equal magnitude; i.e.,

$$Y_J = a \sum_{i=1}^{8} e^{j\phi_i} \tag{18a}$$

where ϕ_i is uniformly distributed on $[0, 2\pi)$. In this situation the maximum instantaneous power of Y_J ($64a^2$) would be only 9 dB above its average power ($8a^2$).

When the amplitudes $a_{J,L,M}$ are fixed, the distribution of $|Y_J|$ is equivalent to the distribution of resultant vector length in a two-dimensional random walk problem where a set number of stops are taken, each of a prescribed length $a_{J,L,M}$ and each in a uniformly random direction $\theta_{J,L}$.

If many steps of constant length are taken in the random walk, or equivalently, if many updates of constant amplitude are summed, then the distribution of the resultant magnitudes approaches a Rayleigh distribution.

Therefore a Rayleigh distribution of $|Y_J|$ can be achieved in either of two ways: 1) by using many updates or 2) by randomizing the magnitudes of the doppler-density matrix elements according to a Rayleigh distribution. (This will be demonstrated in the results section.)

In the following paragraphs the theory of the two-dimensional random walk will be reviewed to provide a basis for calculating the exact statistical nature of the REVGEN output when the amplitudes of the doppler-density matrix are not randomized.

STATISTICS OF MODIFIED REVGEN (Two-Dimensional Random Walk)

In considering the REVGEN statistics of the previous section, it was shown that modification of the original REVGEN concept also alters the statistical nature of the resulting REVGEN output. In effect, the distribution of the magnitude of the output time function $|Y_J|$, as produced by the modified REVGEN described above, is equivalent to the distribution of the resultant vector length in a two-dimensional random walk. Thus the theory to be presented in this section is directly applicable to REVGEN output when the amplitudes of the doppler-density matrix are fixed and the only randomness in Y_J occurs in the random phase angles $\theta_{L,M}$.

Following the theory presented in Rayleigh's "Scientific Papers,"[7] consider the probability that a traveler, after taking n steps of individual lengths $a_1, a_2, \ldots, a_n$, in directions he chose at random, will consequently arrive within a prescribed distance r from his starting point (i.e., $P_n(r; a_1, a_2, \ldots, a_n)$). The direction of his first step is plainly a matter of indifference. On the other hand, at his next $n - 1$ turns, the probability that the angles θ lie within the limits θ_1 and $\theta_1 + d\theta_1$, θ_2 and $\theta_2 + d\theta_2, \ldots \theta_{n-1}$ and $\theta_{n-1} + d\theta_{n-1}$ is

$$\frac{1}{(2\pi)^{n-1}}\, d\theta_1\, d\theta_2 \ldots d\theta_{n-1}. \tag{19}$$

The probability that the resultant vector is less than r is then obtained by integrating the above probability density over only those regions of θ space (an $n-1$ dimensional manifold) for which

$$\left| \sum_{i=1}^{N} a_i e^{j\theta_{i-1}} \right| < r.$$

The evaluation of the multi-dimensional probability integral

$$\left(i.e., P_n(r; a_1, a_2, \ldots a_n) = \frac{1}{(2\pi)^{n-1}} \int_{mag<r} d\theta_1 \, d\theta_2 \ldots d\theta_{n-1} \right) \tag{20}$$

was shown by Kluyver[7] to be equivalent to the following definite integral in one variable. Kluyver's result is

$$P_n(r; a_1, a_2, \ldots a_n) = r \int_0^\infty J_1(rx) J_0(a_1 x) J_0(a_2 x) \ldots J_0(a_n x) \, dx$$

$$= r \int_0^\infty J_1(rx) \, dx \prod_{m=1}^{n} (a_m x) \tag{21}$$

where J_0 and J_1 are respectively the zero and first order Bessel functions.

Thus the problem of obtaining numerical values for the probability, P_n, lies in obtaining a method for accurate numerical evaluation of Kluyver's integral (Equation (21)). The solution of this problem was formulated by Bennett[11] who noted that for the special case of $n = 1$, the problem is trivial; for the case of $n = 2$ it is resolvable in terms of elementary functions; and for the case of n = 3 the problem can be evaluated by elliptical integrals;[10] but for cases of $n > 3$, an alternate method of evaluation is needed. Bennett's results, summarized here, conclude that the probability (P_n) that the magnitude of the resultant vector is less than r, can be calculated using the following convergent Fourier-Bessel series representation:

$$P_n(r; a_1, a_2, \ldots a_n) = 1 - \frac{2}{A} \sum_{m=1}^{\infty} \frac{b_m c_m J_0(r j_m / A)}{j_m J_1^2(j_m)} \tag{22}$$

where j_m is the m^{th} root, in ascending order of magnitude, of the equation $J_0(x) = 0$* and where

$$A = \sum_{m=1}^{n} a_m \tag{23}$$

*See Appendix A for table.

$$b_m = \prod_{s=1}^{n} J_0(a_s j_m / A) \tag{24}$$

$$c_m = \sum_{s=1}^{n} \frac{a_s J_1(a_s j_m / A)}{J_0(a_s j_m / A)} . \tag{25}$$

Or conversely, the probability that the magnitude of the resultant vector will "exceed" r, is 1 minus the probability given in Equation (22), or simply:

$$P_{excess} = \frac{2}{A} \sum_{m=1}^{\infty} \frac{b_m c_m J_0(r j_m / A)}{j_m J_1^2(j_m)} . \tag{26}$$

Returning to the case of the traveling pedestrian, it is known that there exists an absolute limit on the distance he can walk in n steps since each has a prescribed length a_m (the limit being the sum of the lengths of all n steps, occurring when the traveler chooses to walk a straight path). Thus it is impossible for the traveler to reach a distance greater than the sum

$$A = \sum_{m=1}^{n} a_m .$$

Likewise, in Equation (26), for the case where $r = A$, we see that the numerator of the summing term includes the zero order Bessel function evaluated at j_m, which by definition is any value for which $J_0(j_m) = 0$. Thus when r is equal to the limiting value A from Equation (23), the probability that the resultant vector length will be greater than r is zero, yielding precisely the result expected from the preceding paragraph.

From these results, the derived probability distribution for a finite number of steps can now be compared to the Rayleigh distribution with these observations:

1. $\sigma^2 = \frac{1}{2} \sum a_m^2 .$ (27)

2. $E(r^2) = power = 2\sigma^2 = \sum a_m^2 .$ (28)

3. With target component of amplitude A, the signal-to-noise ratio (power)

$$\frac{Power\ target}{Power\ Reverberation} = \frac{A^2}{2\sigma^2} = \frac{A^2}{\sum a_m^2} . \tag{29}$$

In general, this derived probability distribution for the amplitudes of the simulated reverberation return, generated by modified REVGEN, approximates the true Rayleigh distribution with the notable exception that the simulated distribution drops to zero at the point which represents the sum of the component magnitudes. The error introduced by this "drop-off" effect is essentially negligible for large numbers of components, but as the number of significant components (i.e., updates) is reduced, this "drop-off" error becomes increasingly significant. It is this discrepancy, therefore, and its resulting effect on the response of a broadband energy detector, that becomes the subject of discussion in the following section.

RESPONSE OF A BROADBAND ENERGY DETECTOR

The broadband energy detector is one of many types of signal processors available to current sonar systems for analyzing reverberation return. This simple processor examines the envelope of the reverberation time sequence, testing for amplitudes which exceed a predetermined "detection" threshold. Amplitudes which thus exceed the set threshold are sensed and accordingly recorded as target detections. The following section, therefore, examines the statistics of this "detection" response as they apply to the probability theory already presented.

From the first part of the theory section it was shown that for an ocean medium where many scatterers are participating in an instantaneous echo return, the magnitude of the return follows a Rayleigh distribution[4] and when an additional dominant component (e.g., a target) is present in the scattering field, the envelope of the return then follows a Rician distribution.[11] Applying these results to the broadband energy detector, we see that the probability of exceeding a threshold, T, when no target is present (thus recording a false alarm) can be expressed by integrating the equation derived by Rayleigh from T to infinity. Thus the probability of false alarm, PFA, for a given threshold T is

$$PFA = \int_T^\infty \frac{r}{\sigma^2} e^{-r^2/2\sigma^2} dr$$

$$= e^{-r^2/2\sigma^2} \tag{30}$$

Likewise, for the case when there is a target present in the scattering field, the probability that the magnitude of the return will be greater than the threshold, T, (i.e., the probability of detection, PD) is expressed by integrating the Rician function:

$$PD = \int_T^\infty \frac{r}{\sigma^2} e^{-(r^2 + A^2)/2\sigma^2} I_0\left(\frac{rA}{\sigma^2}\right) dr. \tag{31}$$

In general, the above integral, also known as Marcum's Q function, has presented some difficulty in accurate numerical evaluation for non-zero values of A. This problem and methods for its solution have consequently been addressed in a variety of publications, as summarized in Appendix B.

At this point, Equations (30) and (31) provide analytical expressions for the response statistics of the broadband energy detector when it is operating in a fully updated, properly randomized system (i.e., the real world). Likewise, the third theory section has similarly presented a well-defined closed form expression for the probability of exceeding a threshold, T, that applies directly to the simulated REVGEN return when it is operating in its "update" mode. Equation (26) defines the probability of excess applicable to both the condition that no target is present (PFA) and to the condition that there is a dominant "target" component present in the scattering field (PD). When calculating PFA, the sum from Equation (23) includes only the appropriate number of approximately equal scatterer amplitudes, but when using Equation (26) to calculate PD, an additional dominant amplitude component is added to the Equation (23) sum.

Although Equation (26) provides a well-defined representation of the probability statistics for "update" modified REVGEN, when compared to the probability theory of Equations (30) and (31) for a fully updated, properly randomized system, apparent differences warrant consideration of the probability "drop-off" noted earlier. Some questions remain, such as: What effect do the limited update algorithms used to generate the simulated REVGEN output have on the corresponding response of the simple broadband energy detector? and How significant is this effect on the resulting probabilities of false alarm and detection?

Figures 3 and 4 represent graphic comparisons of the "true" Rayleigh distribution and the simulated distribution of REVGEN output generated with 4 updates per pulse length. Both the linear (Figure 3) and the logarithmic (Figure 4) graphs show evidence of the probability "drop-off" previously theorized. When concerned with obtaining values for probabilities of false alarm, we are specifically concerned with the area in the tail of the distribution beyond the value of the detection threshold T. Thus it is clear that for the 4-update simulated REVGEN, as T approaches the drop-off point, the values for PFA drop drastically to zero.

Similarly, Figures 5 and 6 illustrate the same comparisons made in Figures 3 and 4, except that the simulated REVGEN return was, in this case, generated using 8 updates per pulse length. Linearly (Figure 5), this simulated distribution appears to be a much more accurate approximation to the Rayleigh distribution, but the logarithmic scale of Figure 6 shows that although the drop off may not be as readily apparent, it is still present and for higher threshold values, it will still affect the accuracy of probability values thus obtained.

In general, the statistical accuracy of simulated probabilities appears to be greatly influenced by the relative proximity of the detection threshold to the drop-off point for that particular simulation. As the number of updates used to generate the simulated return increases, the value of the drop-off point likewise increases and the error (i.e., the area in the tail of the "true" Rayleigh distribution beyond this point) significantly decreases.

The following section, therefore, will graphically demonstrate the effect of various update algorithms on probability of false alarm statistics, signal-to-noise ratio power curves and receiver operating characteristic curves.

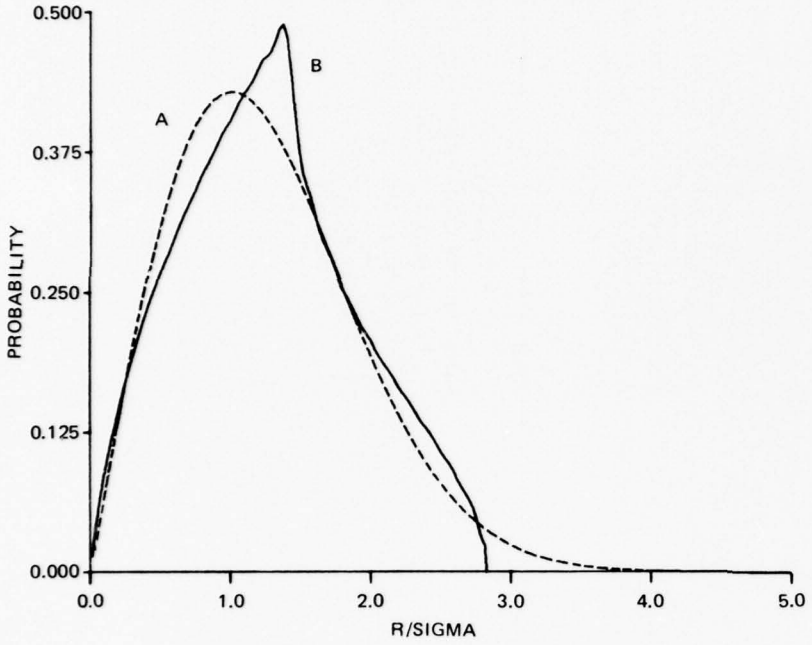

Figure 3. Probability distributions for Rayleigh (A) and 4 updates per pulse length (B).

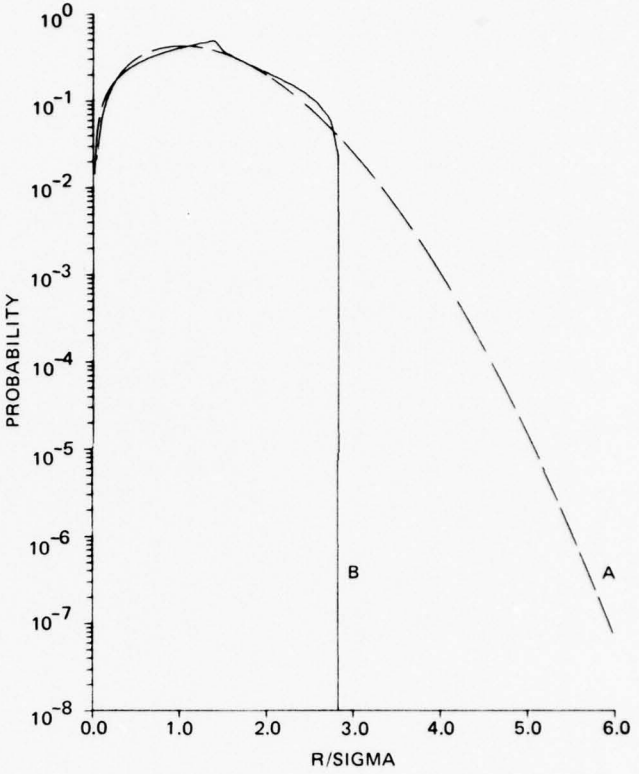

Figure 4. Same as Figure 3 but with logarithmic scale.

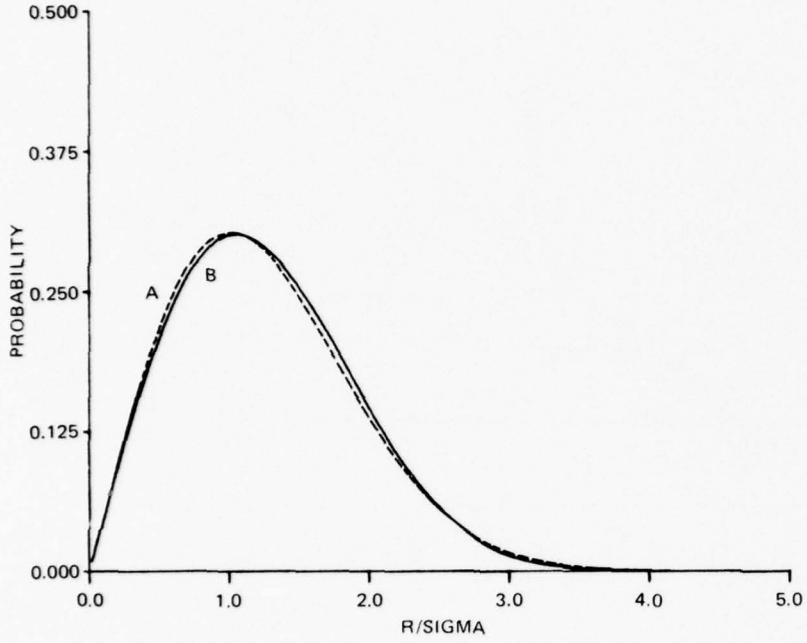

Figure 5. Probability distributions for Rayleigh (A) and 8 updates per pulse length (B).

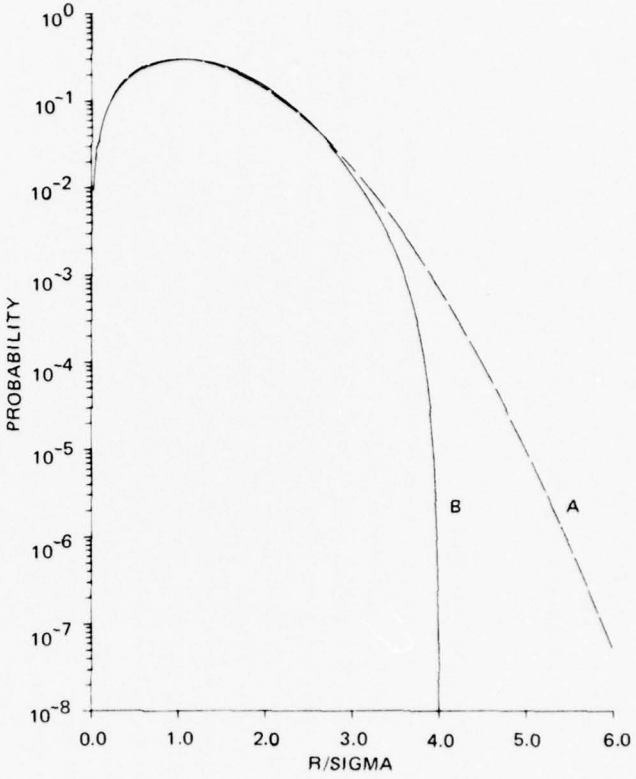

Figure 6. Same as Figure 5 but with logarithmic scale.

RESULTS

This section presents graphic illustrations of the effect of various update algorithms on the probability statistics for simulated REVGEN reverberation return and the corresponding detection statistics as they apply to the various outputs.

PROBABILITY OF FALSE ALARM

The probability that the broadband energy detector will sense a "target" is determined by the probability that the amplitude of the reverberation envelope exceeds a set detection threshold. For REVGEN reverberation returns, the update algorithm incorporated in the simulation places a maximum on the possible amplitude of the return envelope and because there is no possibility of generating amplitudes greater than this limit, correspondingly lowers the probability of false alarm statistics. Figure 7 shows the effect various update algorithms have on their respective PFA curves. For example, at the PFA level of 10^{-3}, an 8-update REVGEN places the detection threshold at approximately 5.8 signal-to-noise power (equivalent to approximately 7.6 dB) while actual Rayleigh statistics indicate the threshold position of 7.0 signal-to-noise power (8.5 dB). Considering this misplaced threshold, the Rayleigh statistics show that this 7.6 dB threshold should yield an actual PFA closer to 10^{-2} rather than the original, erroneously low value of 10^{-3}.

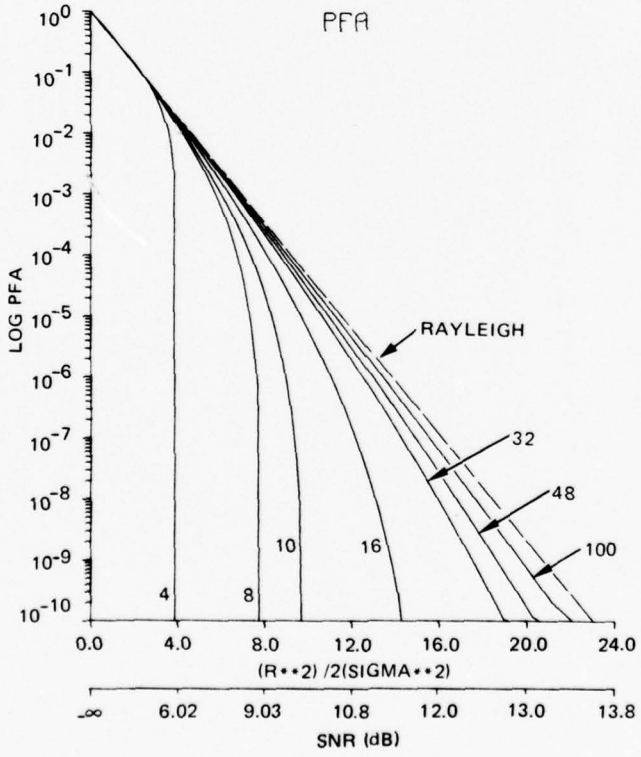

Figure 7. PFA versus threshold for various updates per pulse length; also PFA for Rayleigh distribution.

In addition to the theoretical curves of Figure 7, corresponding experimental data (87,000 samples) were used to generate Figures 8–15. Applying algorithms for 2, 4, and 8 updates per pulse length with fixed amplitudes and random phase, actual REVGEN output yielded the complex time series of the reverberation returns shown in Figures 8–10. For comparison, Figure 11 presents a reverberation envelope generated with both random phase and Rayleigh-distributed amplitudes. Figures 12–15 then use this generated data to lend experimental support to the theoretic probability of false alarm curves from Figure 7.

With a detection threshold set at 3.5 dB, Figures 8–10 illustrate the effect various update algorithms (2, 4, and 8 respectively) have on corresponding false alarm statistics. The apparent amplitude ceiling shown in the return envelopes of Figures 8 and 9 results in unrealistically low PFA rates in both cases. The 8-update algorithm of Figure 10 shows an increase in the "detection" peaks, but in comparison to Figure 12 where 2 updates per pulse length were generated with amplitudes randomized according to a Rayleigh distribution, the number of false alarms for 8 updates of constant amplitude is still erroneously low. The inaccuracies in PFA statistics are reiterated in Figures 12–14, where experimental results are seen to agree with the previously predicted theoretical PFA values. Of particular interest are the experimental results summarized in Figure 15. A simulated reverberation return with update amplitudes randomized according to a Rayleigh distribution is shown to produce the proper PFA statistics independent of update number. (Figure 15 used only 2 Rayleigh randomized updates.)

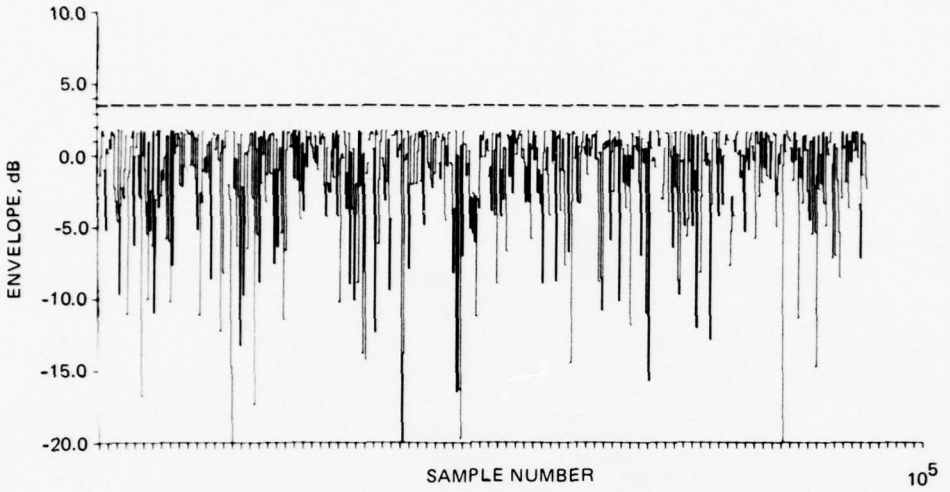

Figure 8. Experimental representation of REVGEN return envelope with 2 updates per pulse length, constant amplitudes, and uniform phase. Detection threshold set at 3.5 dB.

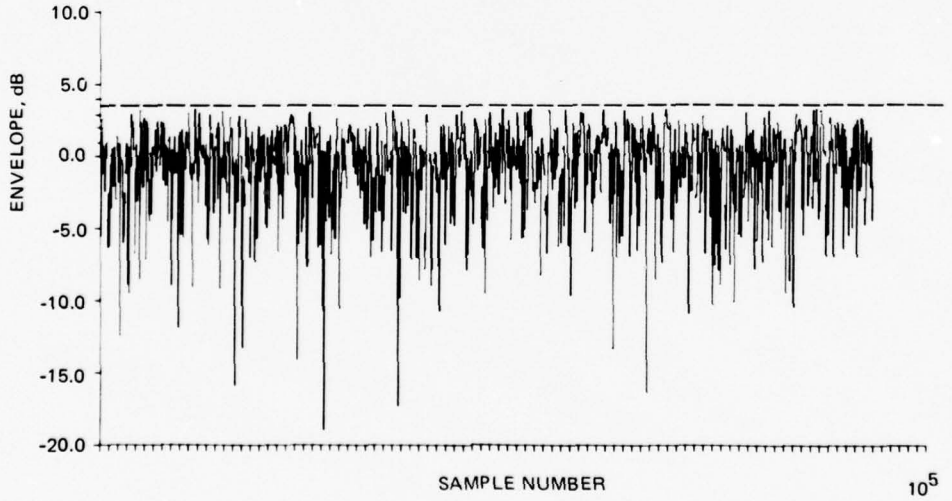

Figure 9. Same as Figure 8 with 4 updates per pulse length.

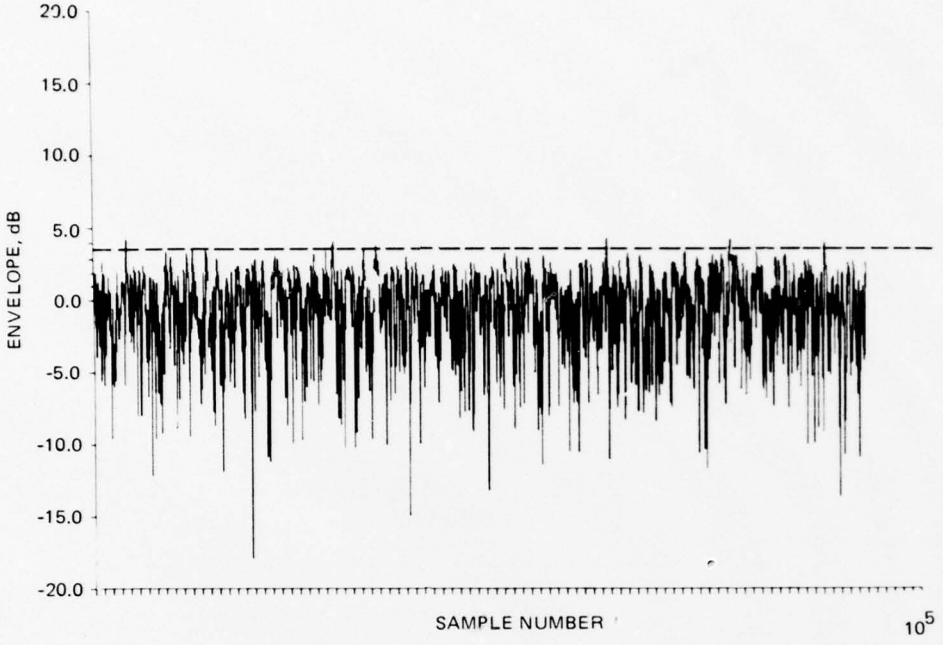

Figure 10. Same as Figure 8 with 8 updates per pulse length.

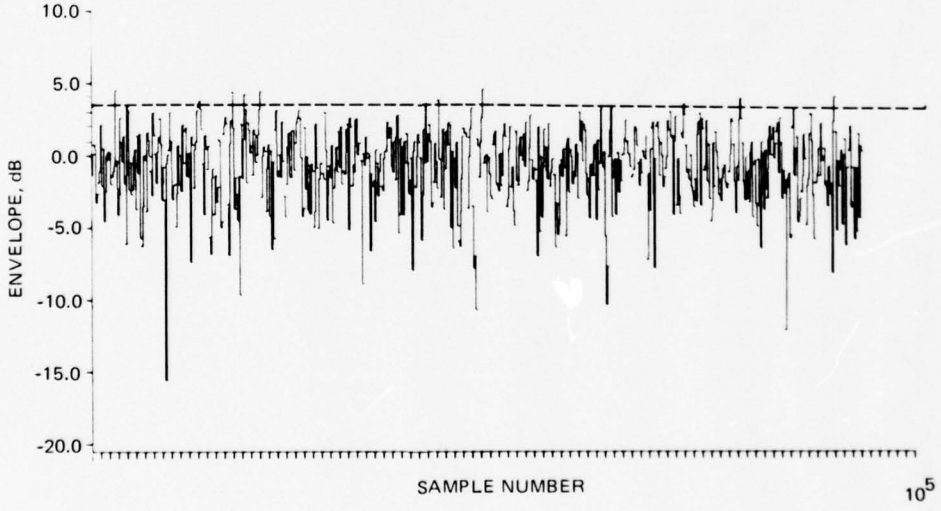

Figure 11. Simulated return envelope with 2 updates per pulse length, uniform phase, but with Rayleigh distributed amplitudes.

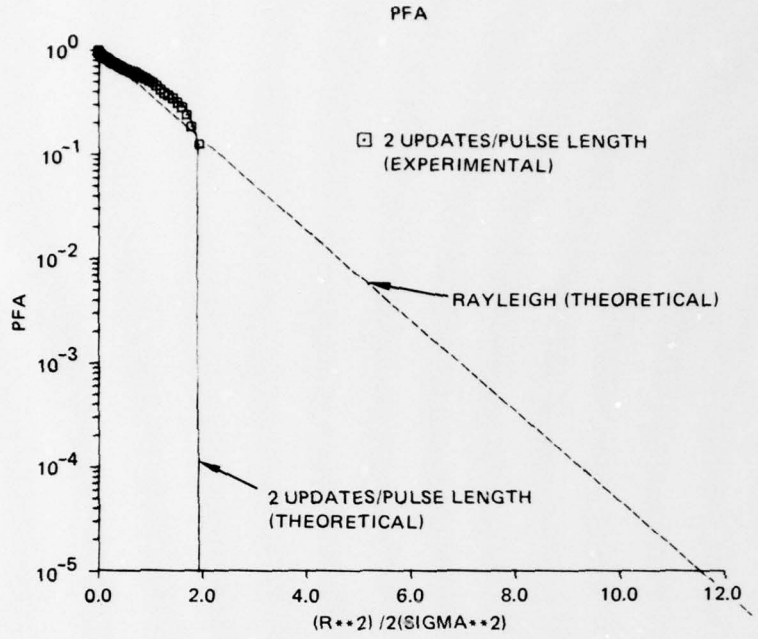

Figure 12. Experimental PFA results (87,000 points in sample) for REVGEN signal with 2 updates per pulse length, constant amplitudes, and uniform phase. Solid lines represent theoretical curves for 2 updates and for Rayleigh.

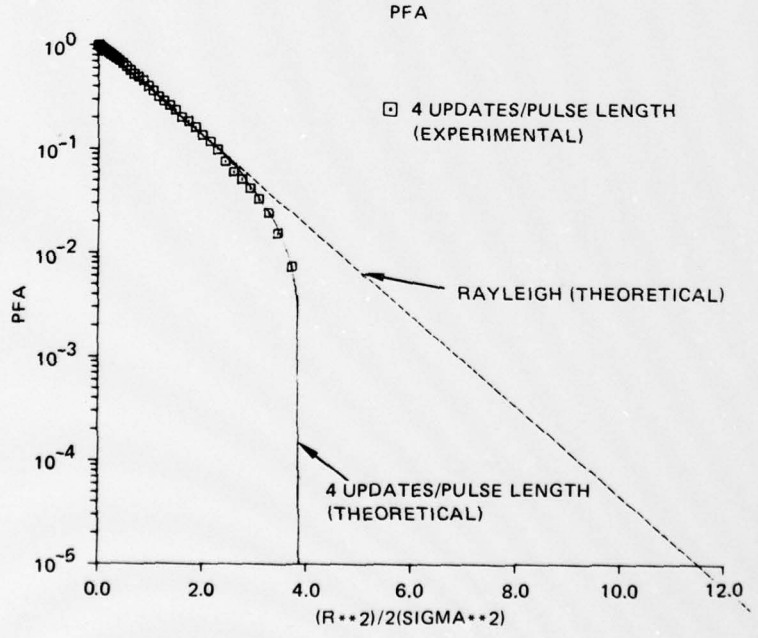

Figure 13. Same as Figure 12 but with 4 updates per pulse length.

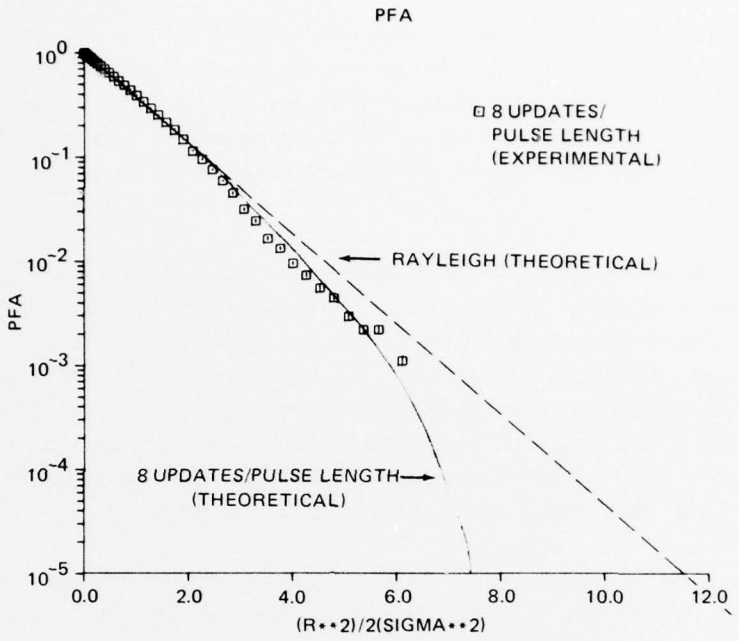

Figure 14. Same as Figure 12 but with 8 updates per pulse length.

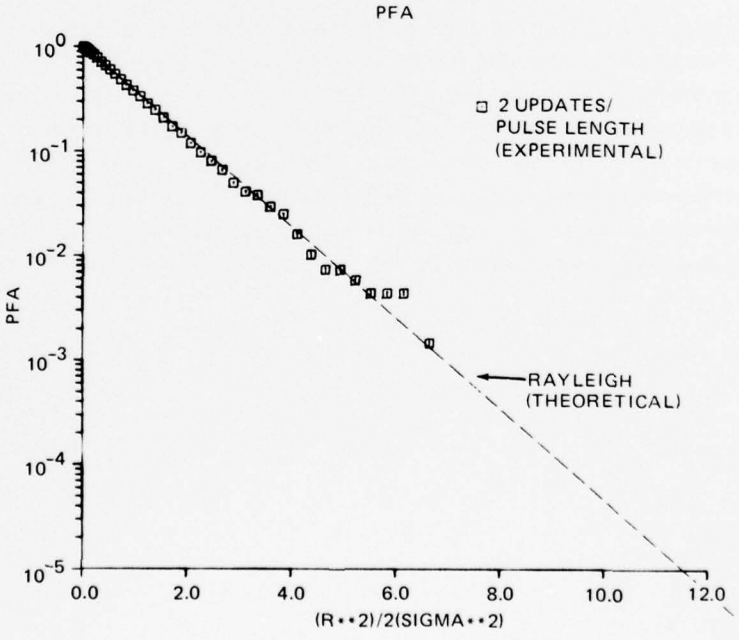

Figure 15. Same as Figure 12 except the update algorithm uses 2 updates per pulse length having Rayleigh distributed amplitudes.

RECEIVER OPERATING CHARACTERISTIC CURVES

Receiver operating characteristic curves graph the probability of false alarm versus the probability of detection for various detection thresholds. As the detection threshold is increased, PFA decreases, but in turn PD also decreases. ROC curves, therefore, are of interest in locating that detection level which provides a maximum PD for a minimum PFA. Figure 16 shows the Rayleigh distribution for noise alone, the Rician distribution with a 10 dB target signal added, and the areas of interest in determining ROC curves (i.e., shaded PFA and striped PD).

Given the altered PFA statistics illustrated in the previous section, it is clear that REVGEN update algorithms will likewise alter the ROC results since the lowered PFA values are used in the ROC comparison of PFA and PD. Figure 17 presents three sets of ROC curves (corresponding to signal-to-noise ratios of 8, 10, and 12 dB) and compares those values obtained by 8 updates per pulse length simulated REVGEN to the actual ROC values from true Rayleigh and Rician distributions. Because the REVGEN PFA drops drastically, Figure 17 shows that for small increments in threshold values near the simulation's implied maximum, PFA decreases rapidly while PD changes only slightly.

For comparison, Figure 18 presents ROC curves similar to Figure 17 but uses a 32-updates-per-pulse-length algorithm. In all three cases, the increased number of updates indicates a closer approximation to the actual Rayleigh/Rician values.

SIGNAL-TO-NOISE RATIO

This third type of graph is similar to the ROC curve in that its main interest lies in the relative accuracy of values obtained for the probability of detection. They differ in that although the previous ROC curves had a fixed signal-to-noise ratio (SNR) and a changing threshold, the following plots set the detection threshold at a predetermined level and vary the signal-to-noise ratio. The focus of Figures 19–21 is to indicate that at various SNR levels, the PD obtained with various versions of REVGEN simulations are erroneously high (the error again due to the stochastic nature of the update algorithms and consequently, to the unreliable values for PFA which cause incorrect placement of the detection threshold).

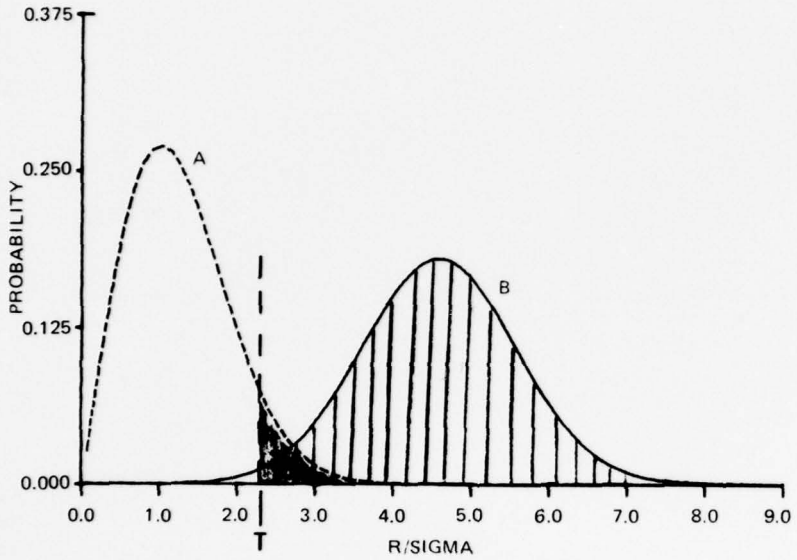

Figure 16. Rayleigh distribution (A) for no target present (shaded area = PFA) and Rician distribution (B) for 10 dB SNR (striped area = PD).

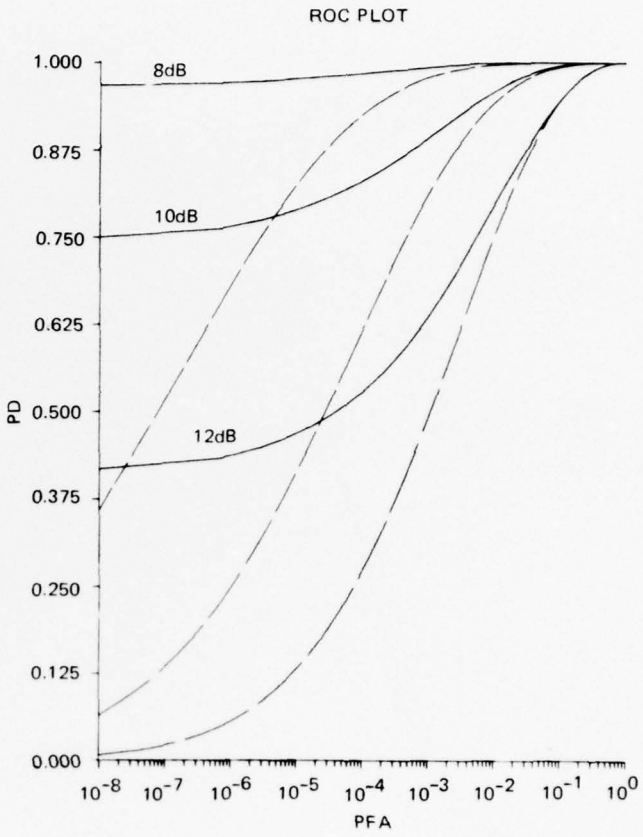

Figure 17. Probability of detection versus probability of false alarm for 8 updates per pulse length and corresponding Rayleigh/Rician curves with SNR fixed at 8, 10, 12 dB.

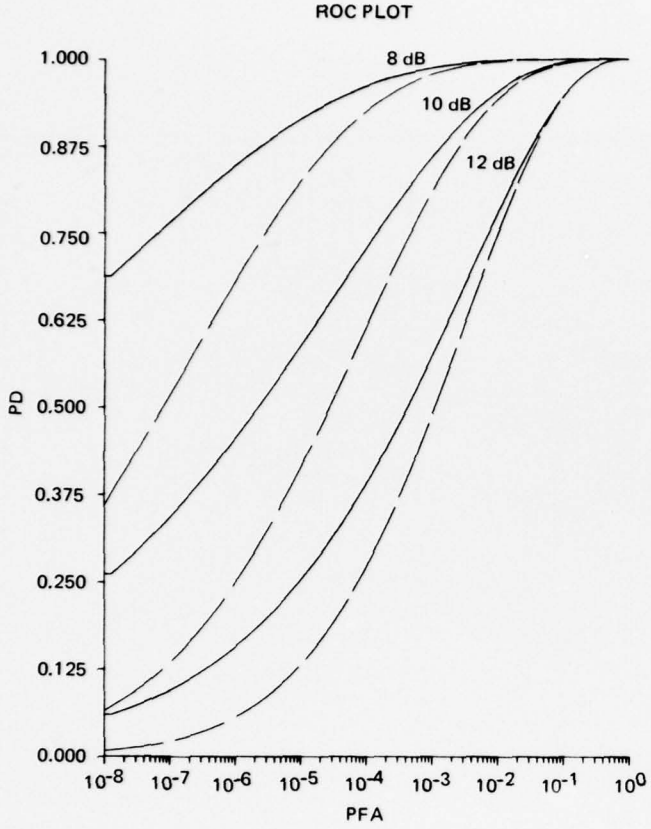

Figure 18. Same as Figure 17 with 32 updates per pulse length.

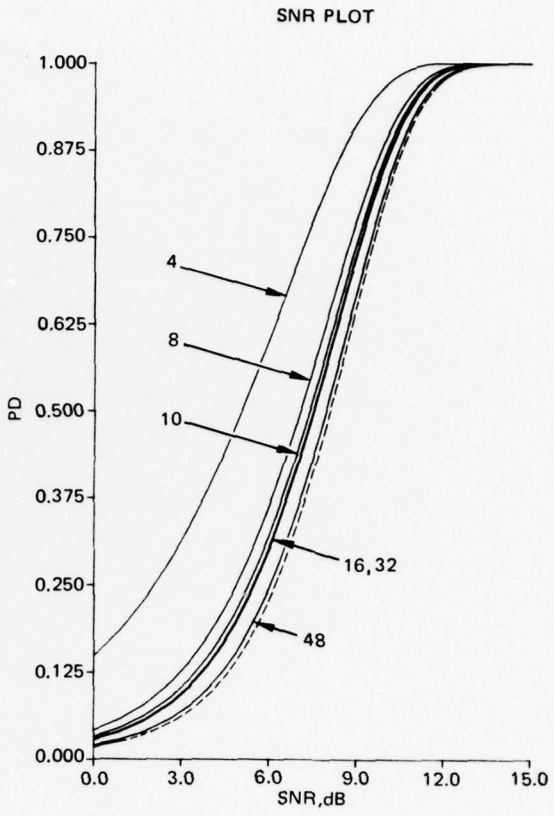

Figure 19. Probability of detection for PFA = 1×10^{-3} as a function of SNR for various update algorithms and for the Rayleigh case.

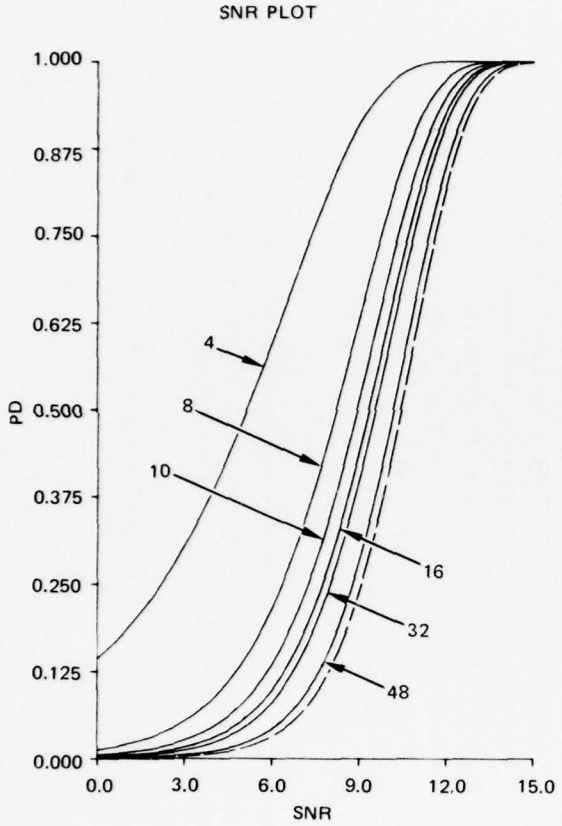

Figure 20. Same as Figure 19 for PFA = 1×10^{-5}.

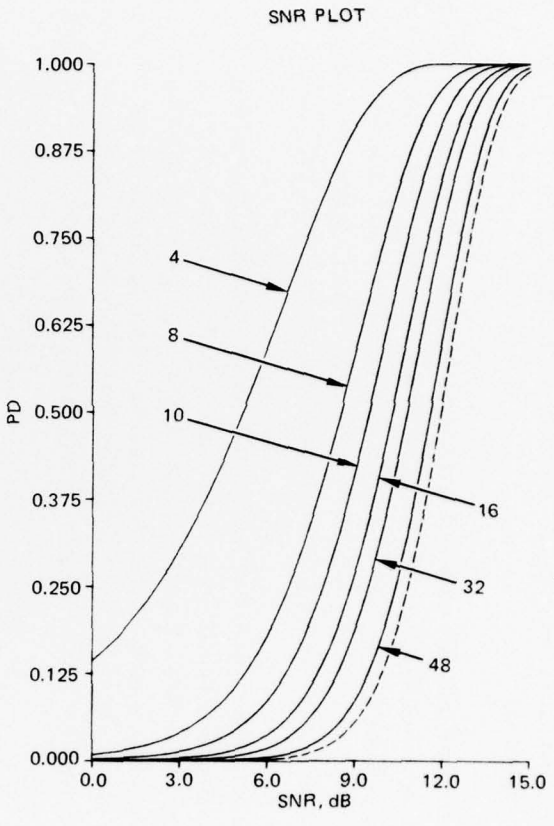

Figure 21. Same as Figure 19 for PFA = 1×10^{-7}.

DISCUSSION

From the preceding section it is seen that both the form of the reverberation signal and the related false alarm and detection statistics can be significantly affected by changes in the update algorithm.

The major effect is the reduction in the probability of high intensity returns in the reverberation signal which occurs when the update magnitudes are held constant. This affects the detection statistics in two ways. First, for a given SNR threshold the probability of false alarm will be less for a signal produced with updates of constant magnitude than for the corresponding signal with updates randomized according to a Rayleigh distribution.

While both theoretical and experimental evidence indicate that increasing the number of updates resolves this disparity, the fact remains that the Rayleigh randomized updates produce the proper statistics (i.e., false alarm and detection statistics for a threshold type energy detector) independent of the update number. This decoupling of the detection statistics from the update algorithm may, in some instances, permit the reduction in REVGEN computational requirements by obviating the need to process a large number of updates per pulse length.

While it has been shown that randomizing the update magnitudes decouples the response of an energy detector from the number of updates used to form the REVGEN signal, it should be concluded that in fact all aspects of the REVGEN time-waveforms become independent of update number when the proper randomization is applied.

Examples of this occur in Figures 22–25 which show the magnitude of the base band reverberation (i.e., envelope of the actual signal) for two pulse shapes and for two different update rates. (In each figure, 5τ of data is plotted.) Figure 22 is calculated for 2 updates per pulse length of Rayleigh distribution. Figure 23 represents a signal for 8 updates per pulse length of uniform phase. Both figures represent the return from a square transmit pulse. For processors which classify detections based on a rapid rise in signal envelope which is followed by a sustained high value for some period of time (e.g., $\tau/2$), a decrease in the number of updates might trigger more false alarms.

Figures 24 and 25 (8 and 2 updates respectively) represent the reverberation return when a Chebyshev window has been applied to the transmit pulse. Under these conditions the envelopes appear more realistic than for the square pulse.

The conclusion to be drawn from these remarks is that when simplifications are made to the optimum Rayleigh simulation (as defined by the pulse length and band width) then a validation is necessary to determine the response of the specific detection logic to the altered signal. In many cases the validation process will result in more efficient algorithms for generating the signal while at the same time insure that the simplification will not alter system performance.

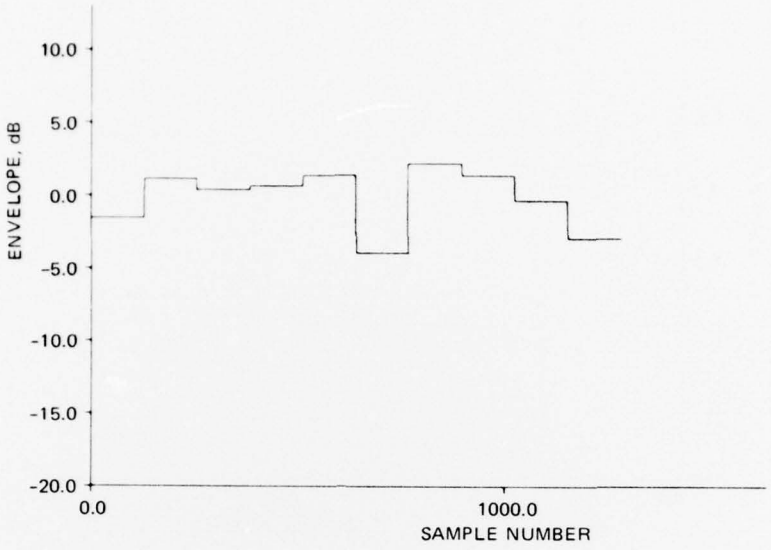

Figure 22. Simulated return envelope with 2 updates per pulse length, uniform phase. Rayleigh distributed amplitudes, and a rectangular transmit pulse. (Samples taken over 5 pulse lengths.)

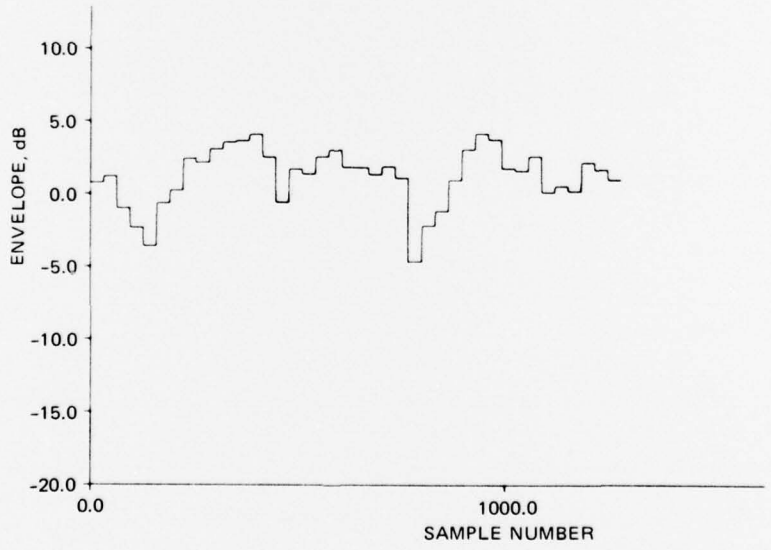

Figure 23. Same as Figure 22 with 8 updates per pulse length and constant amplitudes.

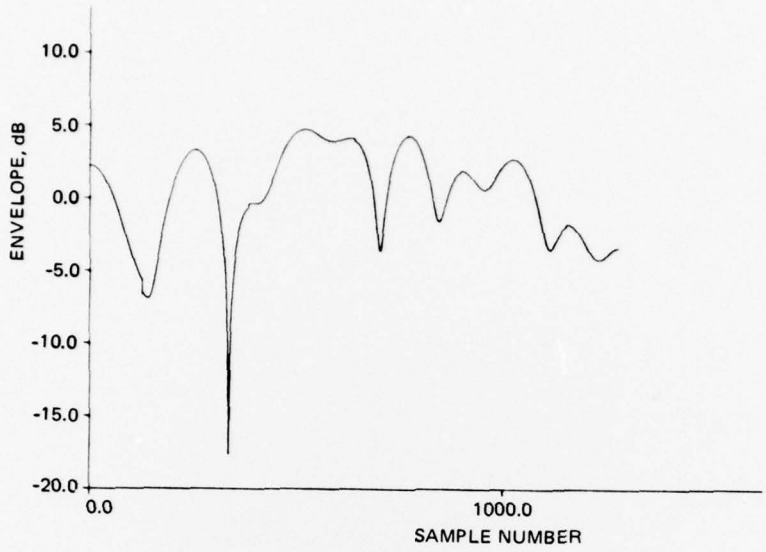

Figure 24. Same as Figure 22 (2 updates, uniform phase, Rayleigh amplitudes) except with a Chebyshev window applied to the transmit pulse.

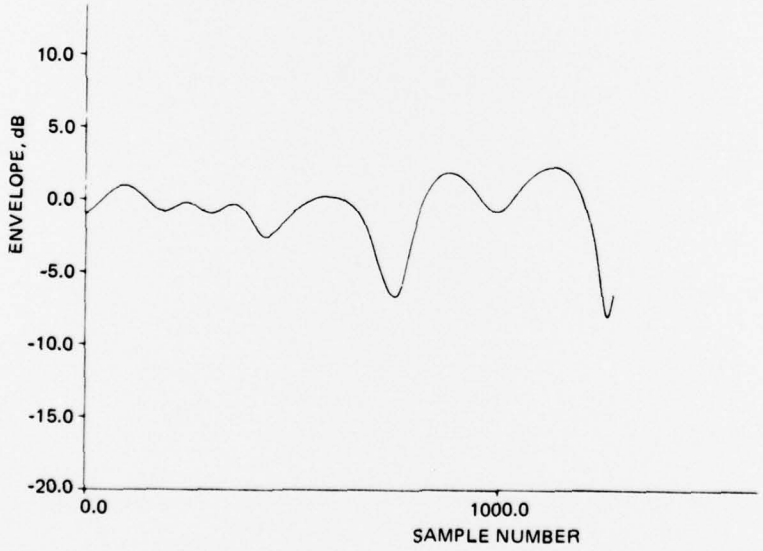

Figure 25. Same as Figure 23 (8 updates, uniform phase, constant amplitudes) except with a Chebyshev window applied to the transmit pulse.

Many current acoustic detectors are based on a matched filter processor. The operation of such a filter is very different from that of a simple energy detector. However, it can be shown that *the statistical problem which must be solved in order to evaluate the effect of the update algorithm is identtical to that presented in the theory section of this report.*

The details of the application of this theory to the problem of a matched filter processor and the effect of various update algorithms is the topic of a future report.

REFERENCES

1. D. W. Princehouse, "REVGEN, A Real-Time Reverberation Generator," Record of the 1977 IEEE International Conference on Acoustics, Speech, and Signal Processing, Catalog No. 77CH1197-3 (Hartford, Conn.), May 1977, pp. 827–835.

2. D. W. Princehouse, "Reverberation Generator Ocean Algorithm, A Status Report," Report No. 7806, Applied Physics Laboratory, University of Washington, February 1978.

3. B. A. Bologna and E. M. Rife, "Real Time Ocean Model for Reverberation," Naval Ocean Systems Center, NOSC TN 383, March 1978.

4. V. V. Ol'shevskii, "Characteristics of Sea Reverberation," Translated from Russian by Consultants Bureau, New York, 1967.

5. M. Schwartz, W. R. Bennett, and S. Stein, "Communication Systems and Techniques," McGraw-Hill, New York, 1966.

6. M. Schwartz, "Information Transmission, Modulation, and Noise," McGraw-Hill, New York, 1970.

7. Rayleigh, "Scientific Papers," Vol. VI, Cambridge University Press, London, 1920.

8. D. W. Princehouse, "REVGEN, A Real-Time Reverberation Generator–Concept Development," Report No. 7511, Applied Physics Laboratory, University of Washington, September 1975.

9. S. O. Rice, "Mathematical Analysis of Random Noise," Bell Systems Technical Journal, Vols. 23 and 24, 1944, 1945.

10. Nicholson, Quarterly Journal of Pure Applied Mathematics, Vol. 48, 1920, pp. 321–329.

11. W. R. Bennett, "Distribution of the Sum of Randomly Phased Components," Quarterly Journal of Pure Applied Mathematics, Vol. 5, January 1948.

APPENDIX A. ZEROS OF THE BESSEL FUNCTION J_0

s	J_0's	s	J_0's
1	2.40482555769577276862163187 9	2	5.52007811028631064959660411 2
3	8.65372791291101221695419871 1	4	11.79153443901428161374304491
5	14.93091770848778594776259399	6	18.07106396791092254314788297
7	21.21163662987925895907839339	8	24.35247153074930273705794481
9	27.49347913204025479587728828	10	30.63460646843197511754957897
11	33.77582021357356868423854639	12	36.91709835366404397976949305
13	40.05842576462823929479930742	14	43.19979171317673035752407277
15	46.34118837166181401868578892	16	49.48260989739781717360276158
17	52.62405184111499602925128542	18	55.76551075501997931168349281
19	58.90698392608094213283440668	20	62.04846919022716988285250031
21	65.18996480020686044063603378	22	68.33146932985679827099230388
23	71.47298160359373282506307389	24	74.61450064370183788382054050
25	77.75602563038805503773937193	26	80.89755587113762786377214353
27	84.03909077693819015787963838	28	87.18062984364115365126180505
29	90.32217263721048005571776680	30	93.46371878194477417119059158
31	96.60526795099626877812161736	32	99.74681985868059647027997904
33	102.88837425419479459642003 47	34	106.02993091645161551017691 76
35	109.17148964980538355206597 75	36	112.31305028049490962749450 66
37	115.45461265366693962811775 71	38	118.59617663087253171562938 49
39	121.73774208795096296523436 29	40	124.87930891323294604525912 88
41	128.02087700600832407976355 98	42	131.16244627521391460789611 54
43	134.30401663830546609935289 73	44	137.44558802028427778778266 19
45	140.58716035285429654848890 28	46	143.72873357368973253395071 84
47	146.87030762579664959413270 53	48	150.01188245695475749088047 34
49	153.15345801922789248759162 60	50	156.29503426853352381954949 57
51	159.43661116426314632349103 83	52	162.57818866894667751905980 94
53	165.71976674795502086669042 72	54	168.86134536923582568745633 79
55	172.00292450307820021540043 19	56	175.14450412190274306537279 83
57	178.28608420007377068148397 41	58	181.42766471373105079421220 00
59	184.56924564063871814111541 17	60	187.71082696004935978007526 62
61	190.85240865258152232178079 94	62	193.99399070010911978994039 72
63	197.13557308566141473621200 31	64	200.27715579333241178336208 79
65	203.41873880819864617124882 07	66	206.56032211624447365545724 54
67	209.70190570429407519748244 71	68	212.84348955994948275074556 61
69	215.98507367153401315699563 83	70	219.12665802804056746518913 14
71	222.26824261908431434128452 48	72	225.40982743485932989851318 24
73	228.55141246609881330119784 11	74	231.69299770403853878097379 66
75	234.83458314038324101980802 37	76	237.97616876727566285555756 38
77	241.11775457726802251499697 15	78	244.25934056329568255880657 66
79	247.40092671865282484808794 11	80	250.54251303696995547044636 57
81	253.68409951219308100469280 89	82	256.82568613856441302431773 32
83	259.96727291060447157306477 80	84	263.10885982309547069270400 30
85	266.25044687106588011884095 47	86	269.39203404977606713817339 66
87	272.53362135470493145351434 89	88	275.67520878153745384789779 54
89	278.81679632615308657846177 43	90	281.95838398461491985431671 01
91	285.09997175315956453913058 82	92	288.24155962818769643811739 54
93	291.38314760625521224168905 05	94	294.52473568406495145823317 75
95	297.66632385845894252404919 06	96	300.80791212641113477166896 93
97	303.94950048502058110605778 02	98	307.09108893150503911477379 74
99	310.23267746319496095259609 35	100	313.37426607752784471969024 55

s	J_0's	s	J_0's
101	316.51585477204292221847752 31	102	319.65744354437615994888734 76
103	322.79903239225555200324754 53	104	325.94062131349668516737048 94
105	329.08221030599855803834302 03	106	332.23379936773963734548991 87
107	335.36538849677413592094340 08	108	338.50697769122849792097948 60
109	341.64856694929807795845225 92	110	344.79015626924400177897536 15
111	347.93174564939019700680817 79	112	351.07333508812058330777196 39
113	354.21492458387641207232872 90	114	357.35651413515374641796625 41
115	360.49810374050107295145694 38	116	363.63969339851703732311190 46
117	366.78128310784829615110604 46	118	369.92287286718747839817743 60
119	373.06446267527124974901834 64	120	376.20605253087847396766713 65
121	379.34764243282846561307990 03	122	382.48923237997932886044652 62
123	385.63082237122637751811959 46	124	388.77241240550063164743456 47
125	391.91400248176738648721140 46	126	395.05559259902484965816206 43
127	398.19718275630284287644780 06	128	401.33877295266156466175501 10
129	404.48036318719041058487776 01	130	407.62195345900684836418159 31
131	410.76354376725534419064153 74	132	413.90513411110633823846514 23
133	417.04672448975526636360825 17	134	420.18831490242162570666570 18
135	423.32990534834808190049664 30	136	426.47149582679961573728320 39
137	429.61308633706270727521922 87	138	432.75467687844455548232461 78
139	435.89626745027233162457130 17	140	439.03785805189246470813345 59
141	442.17944868266995738163914 45	142	445.32103934198773079426595 86
143	448.46263002924599698981678 07	144	451.60422074386165749592797 17
145	454.74581148526772684166574 43	146	457.88740225291277980629414 62
147	461.02899304626042126726195 95	148	464.17058386478877757674420 78
149	467.31217470799000845365438 70	150	470.45376557536983843216339 45
151	473.59535646644710695865007 85	152	476.73694738075333627687923 29
153	479.87853831783231628625330 58	154	483.02012927723970560039750 80
155	486.16172025854264807328480 10	156	489.30331126131940409774578 13
157	492.44490228515899601668600 96	158	495.58649332966086702078684 42
159	498.72808439443455293802282 40	160	501.86967547909936635010781 87
161	505.01126658328409249909412 59	162	508.15285770662669647389647 28
163	511.29444884877404119159269 59	164	514.43604000938161571205416 95
165	517.57763118811327344686574 38	166	520.71922238464097984468494 00
167	523.86081359864456915523651 05	168	527.00240482981150989310934 07
169	530.14399607783667864048177 57	170	533.28558734242214184490841 52
171	536.42717862327694528441198 30	172	539.56876992011691088739023 64
173	542.71036123266444060931891 59	174	545.85195256064832708195317 24
175	548.99354390380357076374475 93	176	552.13513526187120333254054 05
177	555.27672663459811707334750 01	178	558.41831802173690002507560 37
179	561.55990942304567666073587 88	180	564.70150083828795388560805 55
181	567.84309226723247214742933 56	182	570.98468370965306146172084 19
183	574.12627516532850216398680 63	184	577.26786663404239020871801 61
185	580.40945811558300684292816 26	186	583.55104960974319248937110 29
187	586.69264111632022468164885 96	188	589.83423263511569990014348 14
189	592.97582416593541916410861 58	190	596.11741570858927724135568 98
191	599.25900726289115534278087 92	192	602.40059882865881717451757 69
193	605.54219040571380822577899 70	194	608.68378199388135817549022 34
195	611.82537359299028630561101 42	196	614.96696520287290981363190 40
197	618.10855682336495492109781 79	198	621.25014845430547067918611 93
199	624.39174009553674537634977 79		

APPENDIX B

In radar-detection theory and in other problems involving carrier signals, it is often necessary to compute Marcum's Q Function. The Q function is defined as:

$$Q\left(\frac{\mu}{\sigma}, \frac{T}{\sigma}\right) = \int_{T}^{\infty} \frac{r}{\sigma^2} \exp\left[\frac{-(\mu^2 + r^2)}{2\sigma^2}\right] I_0\left(\frac{\mu r}{\sigma^2}\right) dr \qquad \text{(B-1)}$$

or more simply

$$Q(a,b) = \int_{b}^{\infty} x \exp\left[\frac{-(a^2 + x^2)}{2}\right] I_0(ax)\, dx \qquad \text{(B-2)}$$

where I_0 = zero order Bessel function.

While there do exist other asymptotic[1] and recursive[2] formulas for solving the Q function, the recursive method derived by McGee[3] appears to be more accurate and generally the most stable.

This recursive method can be derived by replacing the zero-order Bessel function by its series expansion,

$$I_0(x) = \sum_{n=0}^{\infty} \left(\frac{x}{2}\right)^{2n} \frac{1}{(n!)^2} \qquad \text{(B-3)}$$

inverting the order of summation and integration, and then rearranging the Brennen and Reed summation[2] to be a power series in b instead of in a. Thus we obtain:

$$\begin{aligned} Q(a,b) &= \int_{b}^{\infty} x \exp\left[\frac{-(a^2 + x^2)}{2}\right] I_0(ax)\, dx \\ &= 1 - \int_{0}^{b} x \exp\left[\frac{-(a^2 + x^2)}{2}\right] I_0(ax)\, dx \\ &= 1 - \sum_{k=0}^{\infty} f_k h_k \end{aligned} \qquad \text{(B-4)}$$

where

$$f_o = \left(\frac{b^2}{2}\right) \exp\left(\frac{-b^2}{2}\right)$$

$$h_o = d_o = \exp\left(\frac{-a^2}{2}\right)$$

$$f_k = \frac{\left(\frac{b^2}{2}\right) f_{k-1}}{k-1}$$

$$h_k = h_{k-1} + d_k$$

$$d_k = \frac{\left(\frac{a^2}{2}\right) d_{k-1}}{k}$$

After N iterations, the error in Q is given by the remainder term:

$$E = \sum_{N=1}^{\infty} f_k h_k \tag{B-5}$$

To determine a bound on E, we consider the iterative equations above, which when algebraically substituted within one another, result in:

$$f_{k+1}\, h_{k+1} \leqslant \left[\frac{b^2(2k + a^2)}{4k(k+2)}\right] f_k h_k \tag{B-6}$$

thus giving the ratio of succeeding terms as

$$\frac{f_{k+1}\, h_{k+1}}{f_k h_k} \leqslant \left[\frac{b^2(2k + a^2)}{4k(k+2)}\right] \qquad (k \geqslant 1) \tag{B-7}$$

Note that as k increases, this ratio decreases. Therefore recursive testing for the condition that this ratio of successive terms

$$\left(\frac{f_{k+1}\, h_{k+1}}{f_k h_k}\right) \leqslant \frac{1}{2} \tag{B-8}$$

will then imply that $E \leqslant f_x h_x$.

Thus the summation can be terminated when two conditions are met:

1. The ratio of succeeding terms $\leqslant 1/2$ (implying $E < f_x h_x$)
2. $f_x h_x$ is determined to be an insignificant subtraction from the existing value for Q.

REFERENCES

B-1. C. W. Helstrom, "Statistical Theory of Signal Detection," 2nd ed. New York: Pergamon, 1968, p. 451, eq. F-16.

B-2. L. E. Brennan and I. S. Reed, "A Recursive Method of Computing the Q Function," IEEE Trans. Information Theory (Correspondence), vol. IT-11, April 1965, pg. 312–313.

B-3. W. F. McGee, "Another Recursive Method of Computing the Q Function," IEEE Trans Information Theory (Correspondence), vol. IT-16, July 1970, pg. 500–501.